

Article

First-Principle Study of Rh-Doped Nitrogen Vacancy Boron Nitride Monolayer for Scavenging and Detecting SF₆ Decomposition Products

Zhen Shi ^{1,*} and Sheng-Yuan Xia ² ¹ School of Electrical Engineering, Guangxi University, Nanning 530004, China² State Key Laboratory of Power Transmission Equipment & System Security and New Technology, Chongqing University, Chongqing 400044, China; xiashengyuan@cqu.edu.cn

* Correspondence: z.shi@gxu.edu.cn

Abstract: The scavenging and detection of sulfur hexafluoride (SF₆) decomposition products (SO₂, H₂S, SO₂F₂, SOF₂) critically matters to the stable and safe operation of gas-insulated switchgear (GIS) equipment. In this paper, the Rh-doped nitrogen vacancy boron nitride monolayer (Rh-VNBN) is proposed as a gas scavenger and sensor for the above products. The computational processes are applied to investigate the configurations, adsorption and sensing processes, and electronic properties in the gas/Rh-VNBN systems based on the first-principle calculations. The binding energy (E_b) of the Rh-VNBN reaches -8.437 eV, while the adsorption energy (E_{ad}) and band gap (BG) indicate that Rh-VNBN exhibits outstanding adsorption and sensing capabilities. The density of state (DOS) analysis further explains the mechanisms of adsorption and sensing, demonstrating the potential use of Rh-VNBN in sensors and scavengers of SF₆ decomposition products. This study is meaningful as it explores new gas scavengers and sensors of SF₆ decomposition products to allow the operational status assessment of GIS equipment.

Keywords: high voltage equipment; dielectric material; sulfur hexafluoride (SF₆); defect sensing and scavenging



Citation: Shi, Z.; Xia, S.-Y. First-Principle Study of Rh-Doped Nitrogen Vacancy Boron Nitride Monolayer for Scavenging and Detecting SF₆ Decomposition Products. *Polymers* **2021**, *13*, 3507. <https://doi.org/10.3390/polym13203507>

Academic Editors: M. Tariq Nazir, Shakeel Akram and Yiyi Zhang

Received: 19 August 2021

Accepted: 6 September 2021

Published: 13 October 2021

Publisher's Note: MDPI stays neutral with regard to jurisdictional claims in published maps and institutional affiliations.



Copyright: © 2021 by the authors. Licensee MDPI, Basel, Switzerland. This article is an open access article distributed under the terms and conditions of the Creative Commons Attribution (CC BY) license (<https://creativecommons.org/licenses/by/4.0/>).

1. Introduction

Sulfur hexafluoride (SF₆) is extensively applied in gas-insulated switchgear (GIS) equipment because of its good thermal conductivity, high dielectric strength, ideal arc-extinguishing properties, and chemical inertness [1–3]. Nevertheless, the long-term operation of GIS equipment inevitably results in latent insulation defects that cause partial discharges (PD) [4]. With the effect of PD, SF₆ might decompose into SO₂, H₂S, SO₂F₂, and SOF₂ [5–7]. The decomposition products would cause stronger discharges that would significantly reduce the insulation properties of the SF₆ [8–10]; therefore, the detection of the SF₆ decomposition products is necessary to ensure the reliability of GIS equipment [11,12].

Over the years, considerable attention has been dedicated to two-dimensional (2D) nanomaterials due to their excellent carrier mobility, high chemical activity, and high specific surface area [13–15]. General 2D nanomaterials such as graphene [16–18], boron nitride (BN) [19,20], and transition metal sulfides [21,22] are chemically sensitive materials with excellent performance, which have been researched extensively for gas sensing [23–26]; however, the selectivity is generally not satisfactory to obtain single 2D nanomaterial gas sensors. A variety of nanocomposite materials with a second phase, such as metals [27–30], metal oxides [31–33], and other materials, can be constructed through surface functionalization, thereby improving the sensitivity to certain specific gases. For example, the Rh-BN monolayer has been studied to produce workable SF₆ decomposition gas sensors [34]. Meanwhile, 2D nanomaterials are defective for the most part [35]. The formed electronic variation regions between the defect and pristine material have significant impacts on the

electronic and chemical properties of 2D nanomaterials [36–38]. Moreover, the nitrogen vacancy BN monolayer (VNBN) has better semiconducting properties and thermal stability [39–41]; however, the effects of the vacancy for BN on monitoring SF₆ decomposition products are less well-understood.

In this study, the Rh-doped nitrogen vacancy BN monolayer (Rh-VNBN) is studied as a sensor and scavenger of the SF₆ decomposition products SO₂, H₂S, SO₂F₂, and SOF₂. The relevant theoretical calculations are based on first-principle density functional (DFT) theory. The adsorption and sensing processes of Rh-VNBN for SO₂, H₂S, SO₂F₂, and SOF₂ are calculated and analyzed. The stable configurations of the gas/Rh-VNBN adsorption systems are presented. Moreover, the adsorption energy (E_{ad}), band gap (BG), and electronic properties of these gas/Rh-VNBN adsorption systems are investigated. On this basis, this computational study first presents a gas scavenger and sensor based on Rh-VNBN, which features promising applicability for the scavenging and detection of SF₆ decomposition products, thereby keeping GIS equipment safe and stable during operation.

2. Modeling of the Gas/Rh-VNBN System

2.1. Configurations of Rh-VNBN and Gas Molecules

Figure 1 displays the geometric configurations of pure BN monolayer and SF₆ decomposition gases (SO₂, H₂S, SO₂F₂, SOF₂). As can be seen in Figure 1a, BN exhibits a graphene-like two-dimensional hexagonal layered structure, which contributes to the increase in specific surface area. The bond length between the B atom and N atom is 1.47 Å. As shown in Figure 1b–e, unlike SO₂ and H₂S, SO₂F₂ and SOF₂ have three-dimensional space structures. The high electronegativity and tetrahedral structure make the SO₂F₂ extremely stable, while the physicochemical properties of SOF₂ are similar to SO₂F₂ [42–44].

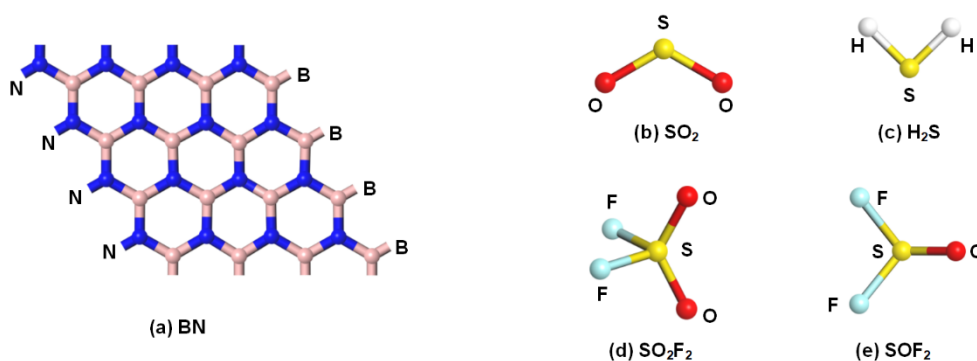


Figure 1. (a) Configurations of pure BN monolayer. (b–e) Configurations of the molecules of SF₆ decomposition products.

The configurations of VNBN and Rh-VNBN after geometric optimization are depicted in Figure 2a,b, respectively. The existence of the nitrogen vacancy (VN) creates additional energy states, as the VN has higher chemical stability as compared with the boron vacancy (VB) [27]. As can be seen in Figure 2b, the Rh atom occupies the VN and bonds to the three adjacent B atoms after doping and geometric optimization. From the front view, the Rh atom bonded to the three B atoms is slightly raised from the VNBN surface.

Generally, the binding energy (E_b) of VNBN is negative after doping with the Rh atom, indicating that there is an exothermic doping process. This also suggests that the doping reaction occurs spontaneously; hence, the doped configurations of Rh-VNBN have higher stability with higher absolute binding energy values. As shown in Figure 2b, high E_b (−8.437 eV) suggests that the Rh atom is stably bonded to VNBN, forming a surface support and strong bonding force in the doping process [45–47]. The above calculation proves that there is a strong interaction between Rh and VNBN and that the Rh-VNBN configurations have high stability.

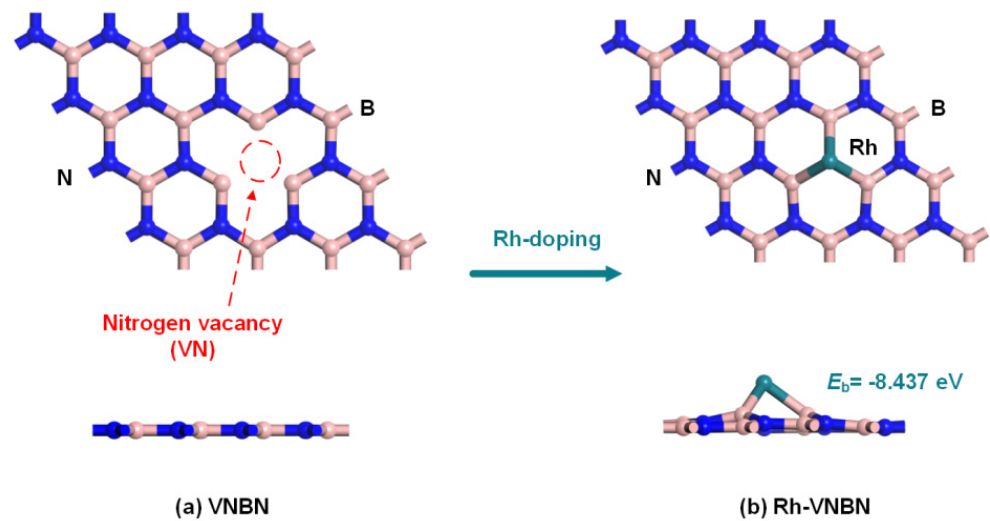


Figure 2. Configurations of the Rh-doped nitrogen vacancy BN monolayer. The red circle represents the nitrogen vacancy. (a) VNBN, (b) Rh-VNBN.

2.2. Electronic Properties of Rh-VNBN

The band structures of the pure BN monolayer and Rh-VNBN are illustrated in Figure 3a,b, respectively. The figure indicates that the band gaps (BG) of the pure BN monolayer and Rh-VNBN are 4.655 eV and 2.892 eV, respectively. The lower band gap of Rh-VNBN indicates that the nitrogen vacancy and doped Rh atom will significantly increase the conductivity and improve the adsorption and sensing properties.

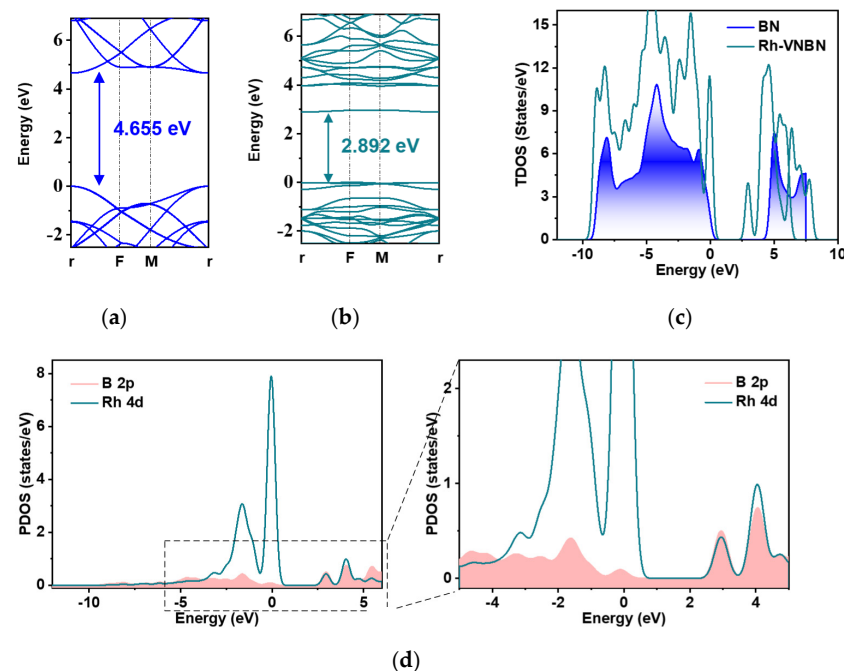


Figure 3. Electronic properties of Rh-VNBN: (a) band structure of pure BN; (b) band structure of Rh-VNBN; (c) TDOS analysis of BN vs. Rh-VNBN; (d) PDOS analysis of Rh-VNBN.

The total density of states (TDOS) and the partial density of states (PDOS) analyses were applied to describe the electronic properties of the nitrogen vacancy BN monolayer after doping with the Rh atom. As shown in Figure 3c, the TDOS of the pure BN monolayer shows notable semiconductor properties, with a band gap at the Fermi level. After doping with the Rh atoms into the nitrogen vacancy, some new states appeared in the TDOS of

the Rh-VNBN at the Fermi level, indicating the nitrogen vacancy and the doped Rh atom contributes obviously to the TDOS. The change in TDOS is consistent with the change in BG, which means that electrons can be easily transferred from the valence band to the conduction band. It can be seen from the PDOS results in Figure 3d that the states of the B 2p orbitals highly overlap with those of the Rh 4d orbital within the range of -5 eV to 5 eV. The above electronic properties suggest strong bonding between the Rh atom and adjacent B atoms in the Rh-VNBN, leading to stable Rh-B bonds and a larger absolute binding energy.

2.3. Configurations of Gas/Rh-VNBN Adsorption Systems

Different configurations of gas/Rh-VNBN pre-adsorption systems are considered in this computational study. Similar to binding energy, the adsorption energy (E_{ad}) of the gas/Rh-VNBN system is generally negative, which corresponds to an exothermic, spontaneous gas adsorption process. With the higher absolute value of E_{ad} , the SF_6 decomposition gases are more easily adsorbed by the Rh-VNBN, which also results in higher stability of the gas/Rh-VNBN adsorption system. After comparing the adsorption energy, the stable systems of various SF_6 decomposition products (SO_2 , H_2S , SO_2F_2 , SOF_2) on Rh-VNBN are displayed in Figure 4. The adsorption distances between Rh-VNBN and various SF_6 decomposition products (SO_2 , H_2S , SO_2F_2 , SOF_2) are 2.289 Å, 2.462 Å, 2.262 Å, and 2.444 Å, respectively. Compared with the pre-adsorption systems, the distance between Rh-VNBN and the SF_6 decomposition gases is shortened, which suggests a tendency of the SF_6 decomposition gases to move toward the Rh-VNBN.

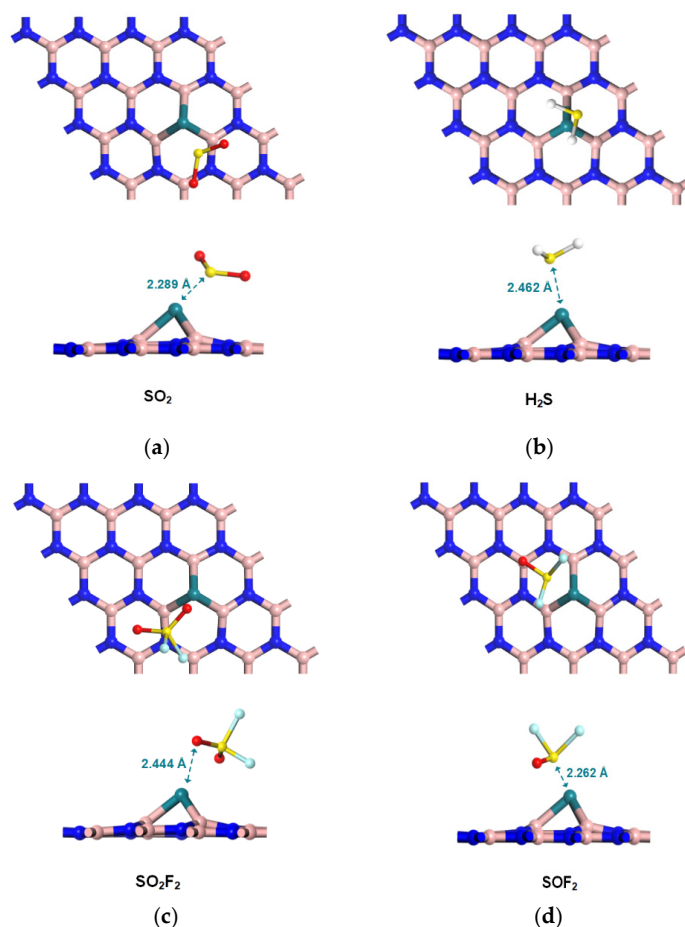


Figure 4. Configurations of gas adsorption systems: (a) SO_2 /Rh-VNBN adsorption system; (b) H_2S /Rh-VNBN adsorption system; (c) SO_2F_2 /Rh-VNBN adsorption system; (d) SOF_2 /Rh-VNBN adsorption system.

3. Results and Discussion

3.1. Adsorption and Sensing Properties of Gas/Rh-VNBN Adsorption System

Figure 5a shows the adsorption energy values of the four gas/Rh-VNBN adsorption systems mentioned above. The adsorption energy values of $\text{SO}_2/\text{Rh-VNBN}$, $\text{H}_2\text{S}/\text{Rh-VNBN}$, $\text{SO}_2\text{F}_2/\text{Rh-VNBN}$, and $\text{SOF}_2/\text{Rh-VNBN}$ adsorption systems are -1.176 eV, -0.911 eV, -0.476 eV, and -1.005 eV, respectively. The adsorption energy of $\text{SO}_2\text{F}_2/\text{Rh-VNBN}$ is lower than the other three adsorption systems and is physically absorbed by the Rh-VNBN. This indicates that the $\text{SO}_2\text{F}_2/\text{Rh-VNBN}$ adsorption system is not as stable as the other three adsorption systems; however, it is important that the adsorption processes of SF6 decomposition products in Rh-VNBN are all spontaneous and stable.

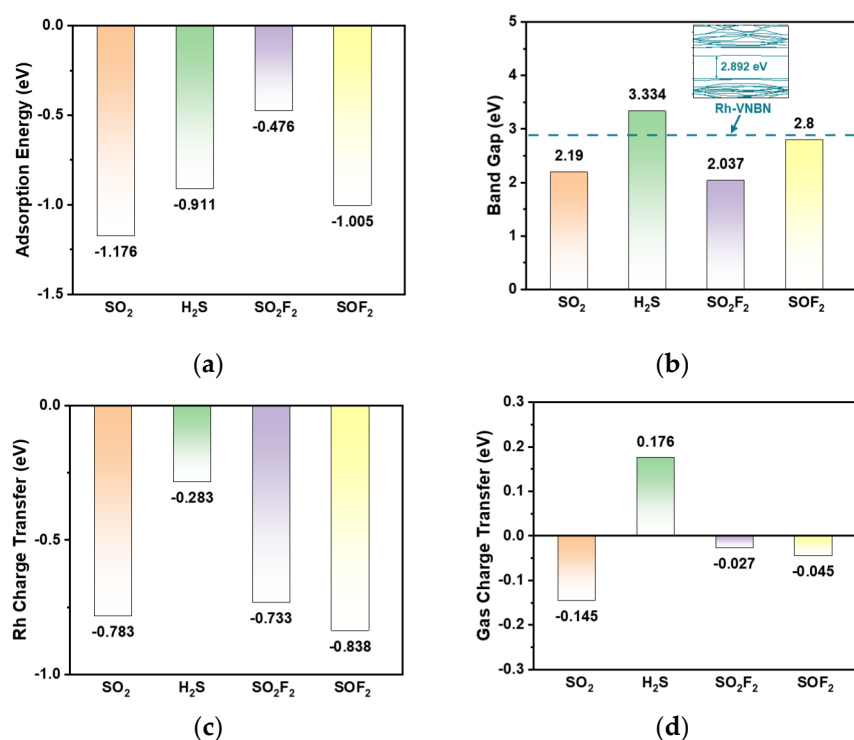


Figure 5. Adsorption and sensing properties of the gas/Rh-VNBN adsorption system: (a) E_{ad} values of the four gas/Rh-VNBN adsorption systems; (b) band gap values of the four gas/Rh-VNBN adsorption systems; (c) charge transfer values of the Rh atom in the four gas/Rh-VNBN adsorption systems; (d) charge transfer values of the gas molecules in the four gas/Rh-VNBN adsorption systems.

As presented in Figure 5b, the BG values of $\text{SO}_2/\text{Rh-VNBN}$, $\text{H}_2\text{S}/\text{Rh-VNBN}$, $\text{SO}_2\text{F}_2/\text{Rh-VNBN}$, and $\text{SOF}_2/\text{Rh-VNBN}$ adsorption systems are 2.190 eV, 3.334 eV, 2.037 eV, and 2.800 eV, respectively. Moreover, the sensing analysis of the gas/Rh-VNBN adsorption systems is based on the changes of resistance. It is well known that the greater the change in BG, the greater the change in conductivity (σ) of the gas/Rh-VNBN system. As the resistance and σ are negatively correlated, the sensing properties of Rh-VNBN for SO_2 , H_2S , and SO_2F_2 are consequently better than those for SOF_2 .

In addition, the Rh charge transfer (Q_{Rh}) and Gas charge transfer (Q_{gas}) based on the Mulliken population analysis are shown in Figure 5c,d, respectively. The charge transfer values of the Rh atom in the $\text{SO}_2/\text{Rh-VNBN}$, $\text{H}_2\text{S}/\text{Rh-VNBN}$, $\text{SO}_2\text{F}_2/\text{Rh-VNBN}$, and $\text{SOF}_2/\text{Rh-VNBN}$ adsorption systems are -0.783 eV, -0.283 eV, -0.733 eV, and -0.838 eV, respectively. The Q_{Rh} is negative in all four adsorption systems, indicating that Rh atom always loses electrons during the adsorption process. In Figure 5d, the charge transfer values of the gas molecules in the $\text{SO}_2/\text{Rh-VNBN}$, $\text{H}_2\text{S}/\text{Rh-VNBN}$, $\text{SO}_2\text{F}_2/\text{Rh-VNBN}$ and $\text{SOF}_2/\text{Rh-VNBN}$ adsorption systems are -0.145 eV, 0.176 eV, -0.027 eV, and -0.045 eV,

respectively. The Q_{gas} is negative for all adsorption systems except the $\text{SO}_2/\text{Rh-VNBN}$ adsorption system. This indicates that electrons are transferred from gases to Rh-VNBN during the adsorption process for most of the SF_6 decomposition products (H_2S , SO_2F_2 , SOF_2).

3.2. Electronic Properties and Mechanisms of the Gas/Rh-VNBN Adsorption Systems

The TDOS and PDOS analyses for various gas adsorption systems are used for in-depth investigation of the electronic properties of gas/Rh-VNBN adsorption systems to elucidate sensing and adsorption mechanisms. As presented in Figure 6, except for the $\text{H}_2\text{S}/\text{Rh-VNBN}$ adsorption system, the TDOS values near the Fermi level in the other adsorption systems shift slightly to the left, with more electrons appearing between the valence band and conduction band. As such, most of the adsorption is beneficial to the conductivity of the gas/Rh-VNBN systems; however, the conductivity of the $\text{H}_2\text{S}/\text{Rh-VNBN}$ adsorption systems decreases slightly, which is consistent with the change of the band gap.

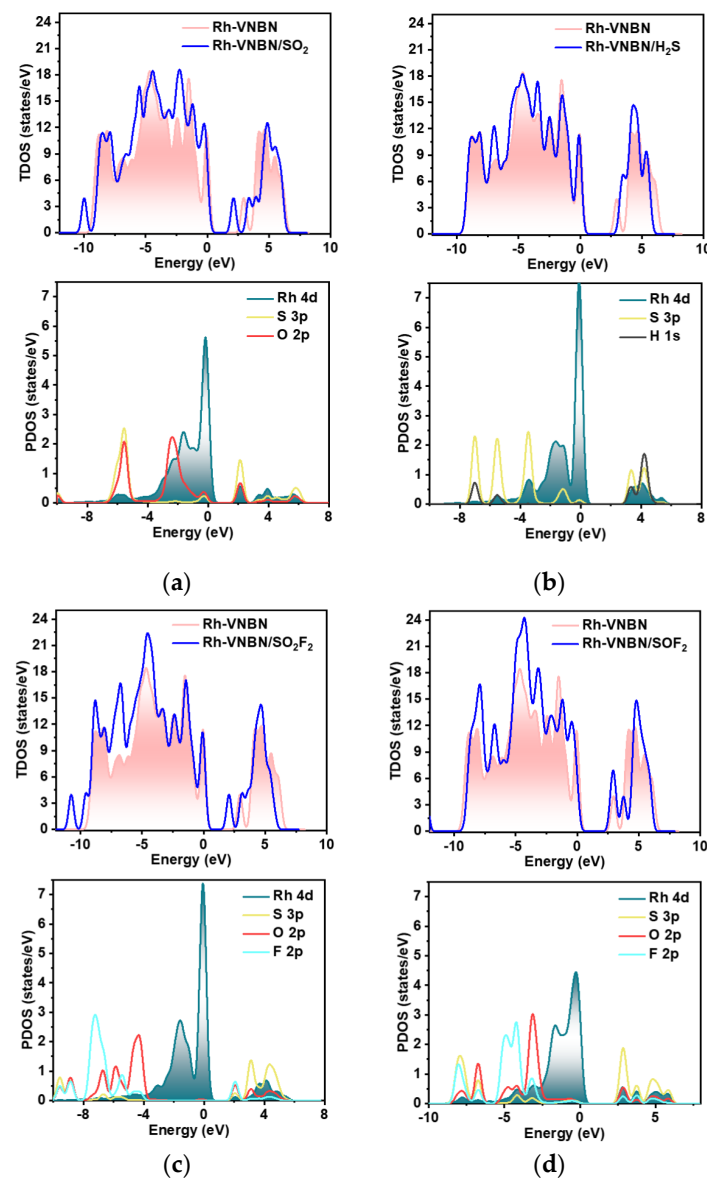


Figure 6. TDOS and PDOS analyses of gas/Rh-VNBN adsorption systems: (a) $\text{SO}_2/\text{Rh-VNBN}$ adsorption systems; (b) $\text{H}_2\text{S}/\text{Rh-VNBN}$ adsorption systems; (c) $\text{SO}_2\text{F}_2/\text{Rh-VNBN}$ adsorption systems; (d) $\text{SOF}_2/\text{Rh-VNBN}$ adsorption systems.

From the perspective of PDOS, the Rh orbital in the $\text{SO}_2\text{F}_2/\text{Rh-VNBN}$ adsorption system has relatively little overlap with the frontier atom orbitals of the gas molecule compared to the other three systems; therefore, the Rh 4d orbital is less hybridized with S 3p, O 2p, and F 2p of SO_2F_2 . This suggests that the bonding force between Rh-VNBN and SO_2F_2 is not as strong as the other three gases (SO_2 , H_2S , SOF_2). The PDOS explains why the adsorption energy absolute value of $\text{SO}_2\text{F}_2/\text{Rh-VNBN}$ is higher than the other three adsorption systems. Moreover, the Rh 4d orbital is strongly hybridized with frontier atom orbitals of SO_2 , H_2S , and SOF_2 gas molecules, demonstrating that the bonding force between Rh-VNBN and these three gases is strong. Correspondingly, the PDOS also illustrates that most gas/Rh-VNBN adsorption systems in this study are stable. In summary, the DOS values of gas/Rh-VNBN adsorption systems also further illustrate the potential of Rh-VNBN in sensors and scavengers of SF_6 -decomposed products.

4. Conclusions

In this study, Rh-VNBN is proposed for the scavenging and detection of SF_6 -decomposed products. First-principle calculations based on DFT theory are applied to study the configurations, adsorption and sensing process, and electronic properties of Rh-VNBN for SF_6 -decomposed products. The following conclusions are drawn from the present study.

The Rh atom occupies the nitrogen vacancy and bonds to the three adjacent B atoms to form a stable configuration of Rh-VNBN. The binding energy (E_b) of Rh-VNBN reaches -8.437 eV, indicating that the Rh atom is stably bonded to VNBN. Moreover, the nitrogen vacancy and doped Rh atom significantly improve the conductivity of Rh-VNBN.

1. Based on the analysis of the adsorption energy (E_{ad}), the adsorption processes of SF_6 decomposition products on Rh-VNBN are spontaneous and stable. In addition, the changes of the band gap (BG) suggest the sensing properties of Rh-VNBN for SO_2 , H_2S , and SO_2F_2 are better than that for SOF_2 . Rh-VNBN exhibits outstanding adsorption and sensing capabilities for various SF_6 -decomposed gases;
2. The electronic properties of gas/Rh-VNBN systems are studied, contributing to the understanding of the adsorption and sensing mechanisms. Additionally, the DOS further demonstrates the potential of Rh-VNBN for use in sensors and scavengers of SF_6 -decomposed products;
3. From a long-term perspective, this computational study on gas/Rh-VNBN adsorption systems is important for future research on scavengers and sensors of SF_6 -decomposed gases, thereby ensuring the safe and stable operation of GIS equipment.

5. Computational Details

All of the first-principle calculations were performed using the DMol³ package in Materials Studio (MS) based on DFT [48], which has been demonstrated to be reasonable in previous experimental and theoretical studies [15,49–52]. The electron exchange and correlation process was set to the generalized gradient approximation (GGA) of the Perdew–Burke–Ernzerhof (PBE) functional [53]. The double numerical basis with polarization (DNP) was used as the atomic orbital basis set, while the DFT semi-core pseudopotential (DSSP) was applied to process the relativistic effects of the Rh atom [54]. Considering the van der Waals forces of the gases and Rh-VNBN, the semi-empirical dispersion corrections (DFT-D) method proposed by Grimme was applied to better investigate long-range weak interactions [55]. The pure BN monolayer supercell, including 16 B and 16 N atoms, was built with a graphene-like structure. The k-point sample of the Monkhorst–Pack grid was sampled as $8 \times 8 \times 1$ and $5 \times 5 \times 1$ for electronic structure and geometry optimization calculations, respectively [56]. The convergence criteria adopted in this study, including the energy tolerance accuracy, maximum force, and maximum displacement, were set as 10^{-5} Ha, 2×10^{-3} Ha/Å, and 5×10^{-3} Å, respectively [57]. For static electronic structure calculations, a self-consistent loop energy of 10^{-6} Ha, global orbital cutoff radius of 5.0 Å, and smearing of 5×10^{-3} Ha were applied [30].

To identify the doping site of the nitrogen vacancy BN monolayer with the best stability, various Rh doping sites were considered and analyzed. In general, the binding energy (E_b) of Rh-VNBN is adopted to assess the doping stability of the Rh atom. The E_b is determined using Formula (1) as presented below:

$$E_b = E_{\text{Rh-VNBN}} - E_{\text{Rh}} - E_{\text{VNBN}} \quad (1)$$

where $E_{\text{Rh-VNBN}}$, E_{Rh} , and E_{VNBN} are the energy of the Rh-VNBN, Rh atom, and nitrogen vacancy BN monolayer, respectively.

Similarly, to identify the best stability of geometric configurations for SF_6 decomposition gases (SO_2 , H_2S , SO_2F_2 , SOF_2) adsorbed on the Rh-VNBN, the adsorption energy (E_{ad}) of the gas/Rh-VNBN adsorption system is commonly applied to assess adsorption properties. The E_{ad} is calculated using the following formula:

$$E_{\text{ad}} = E_{\text{gas/Rh-VNBN}} - E_{\text{Rh-VNBN}} - E_{\text{gas}} \quad (2)$$

where $E_{\text{gas/Rh-VNBN}}$, $E_{\text{Rh-VNBN}}$, and E_{gas} represent the total energy of the gas/Rh-VNBN adsorption system, isolated Rh-VNBN, and gas molecule, respectively.

Depending on the variation of the band gap (BG), the relevant conductivity (σ) changes of gas/Rh-VNBN system can be calculated using Formula (3):

$$\sigma \propto \exp(-\text{BG}/2kT) \quad (3)$$

where T is the temperature in kelvin (K).

Author Contributions: Formal analysis, Z.S.; Investigation, Z.S.; Methodology, Z.S.; Software, S.-Y.X.; Writing—original draft, S.-Y.X.; Writing—review & editing, Z.S. Both authors have read and agreed to the published version of the manuscript.

Funding: This work is supported by the Sichuan Provincial Science and Technology Key R&D Project (2021YFG0199).

Institutional Review Board Statement: Not applicable.

Informed Consent Statement: Not applicable.

Conflicts of Interest: The authors declare no conflict of interest.

References

- Cui, H.; Zhang, X.; Zhang, J.; Zhang, Y. Nanomaterials-based gas sensors of SF_6 decomposed species for evaluating the operation status of high-voltage insulation devices. *High Volt.* **2019**, *4*, 242–258. [[CrossRef](#)]
- Liu, D.; Gui, Y.; Ji, C.; Tang, C.; Zhou, Q.; Li, J.; Zhang, X. Adsorption of SF_6 decomposition components over Pd (1 1 1): A density functional theory study. *Appl. Surf. Sci.* **2019**, *465*, 172–179. [[CrossRef](#)]
- Qian, H.; Deng, J.; Xie, Z.; Pan, Z.; Zhang, J.; Zhou, H. Adsorption and Gas Sensing Properties of the $\text{Pt}_3\text{-MoSe}_2$ Monolayer to SOF_2 and SO_2F_2 . *ACS Omega* **2020**, *5*, 7722–7728. [[CrossRef](#)] [[PubMed](#)]
- Liu, M. Adsorption Behavior of Ni-Doped ZnO Monolayer upon SF_6 Decomposed Components and Effect of the Applied Electric Field. *ACS Omega* **2020**, *5*, 24118–24124. [[CrossRef](#)] [[PubMed](#)]
- Singh, A.; Bae, H.; Lee, S.; Shabbiri, K.; Hussain, T.; Lee, H. Highly sensitive and selective sensing properties of modified green phosphorene monolayers towards SF_6 decomposition gases. *Appl. Surf. Sci.* **2020**, *512*, 145641. [[CrossRef](#)]
- Tang, J.; Liu, F.; Zhang, X.; Meng, Q.; Zhou, J. Partial discharge recognition through an analysis of SF_6 decomposition products part 1: Decomposition characteristics of SF_6 under four different partial discharges. *IEEE Trans. Dielectr. Electr. Insul.* **2012**, *19*, 29–36. [[CrossRef](#)]
- Tang, J.; Liu, F.; Zhang, X.; Meng, Q.; Zhou, J.; Tao, J. Partial discharge recognition through an analysis of SF_6 decomposition products part 2: Feature extraction and decision tree-based pattern recognition. *IEEE Trans. Dielectr. Electr. Insul.* **2012**, *19*, 37–44. [[CrossRef](#)]
- Koch, H.; Goll, F.; Magier, T.; Juhre, K. Technical aspects of gas insulated transmission lines and application of new insulating gases. *IEEE Trans. Dielectr. Electr. Insul.* **2018**, *25*, 1448–1453. [[CrossRef](#)]
- Hyrenbach, M.; Zache, S. Alternative insulation gas for medium-voltage switchgear. In Proceedings of the 2016 Petroleum and Chemical Industry Conference Europe (PCIC Europe), Berlin, Germany, 14–16 June 2016; pp. 1–9.

10. Zhang, X.; Chen, Z.; Chen, D.; Cui, H.; Tang, J. Adsorption behaviour of SO₂ and SOF₂ gas on Rh-doped BNNT: A DFT study. *Mol. Phys.* **2020**, *118*, e1580394. [[CrossRef](#)]
11. Wang, D.W.; Wang, X.H.; Yang, A.J.; Chu, J.F.; Lv, P.L.; Liu, Y.; Rong, M.Z. MoTe₂: A Promising Candidate for SF₆ Decomposition Gas Sensors with High Sensitivity and Selectivity. *IEEE Electron Device Lett.* **2018**, *39*, 292–295. [[CrossRef](#)]
12. Sun, H.; Gui, Y.; Wei, H.; Long, Y.; Wang, Q.; Tang, C. DFT study of SF₆ decomposed products on Pd–TiO₂: Gas sensing mechanism study. *Adsorption* **2019**, *25*, 1643–1653. [[CrossRef](#)]
13. Zhou, Q.; Ju, W.; Su, X.; Yong, Y.; Li, X. Adsorption behavior of SO₂ on vacancy-defected graphene: A DFT study. *J. Phys. Chem. Solids* **2017**, *109*, 40–45. [[CrossRef](#)]
14. Bhimanapati, G.R.; Lin, Z.; Meunier, V.; Jung, Y.; Cha, J.; Das, S.; Xiao, D.; Son, Y.; Strano, M.S.; Cooper, V.R.; et al. Recent Advances in Two-Dimensional Materials beyond Graphene. *ACS Nano* **2015**, *9*, 11509–11539. [[CrossRef](#)]
15. Zhang, X.; Yu, L.; Wu, X.; Hu, W. Experimental Sensing and Density Functional Theory Study of H₂S and SOF₂ Adsorption on Au-Modified Graphene. *Adv. Sci.* **2015**, *2*, 1500101. [[CrossRef](#)] [[PubMed](#)]
16. Sun, Z.; Chang, H. Graphene and Graphene-like Two-Dimensional Materials in Photodetection: Mechanisms and Methodology. *ACS Nano* **2014**, *8*, 4133–4156. [[CrossRef](#)]
17. Xu, M.; Liang, T.; Shi, M.; Chen, H. Graphene-Like Two-Dimensional Materials. *Chem. Rev.* **2013**, *113*, 3766–3798. [[CrossRef](#)] [[PubMed](#)]
18. Yoon, H.J.; Jun, D.H.; Yang, J.H.; Zhou, Z.; Yang, S.S.; Cheng, M.M.-C. Carbon dioxide gas sensor using a graphene sheet. *Sens. Actuators B Chem.* **2011**, *157*, 310–313. [[CrossRef](#)]
19. Wang, H.; Taychatanapat, T.; Hsu, A.; Watanabe, K.; Taniguchi, T.; Jarillo-Herrero, P.; Palacios, T. BN/Graphene/BN Transistors for RF Applications. *IEEE Electron Device Lett.* **2011**, *32*, 1209–1211. [[CrossRef](#)]
20. Jain, N.; Bansal, T.; Durcan, C.; Yu, B. Graphene-Based Interconnects on Hexagonal Boron Nitride Substrate. *IEEE Electron Device Lett.* **2012**, *33*, 925–927. [[CrossRef](#)]
21. Huang, X.-Y.; Chi, Z.-T.; Liu, J.; Li, D.-H.; Sun, X.-J.; Yan, C.; Wang, Y.-C.; Li, H.; Wang, X.-D.; Xie, W.-F. Enhanced gas sensing performance based on p-NiS/n-In₂O₃ heterojunction nanocomposites. *Sens. Actuators B Chem.* **2020**, *304*, 127305. [[CrossRef](#)]
22. Liu, J.; Hu, Z.; Zhang, Y.; Li, H.-Y.; Gao, N.; Tian, Z.; Zhou, L.; Zhang, B.; Tang, J.; Zhang, J.; et al. MoS₂ Nanosheets Sensitized with Quantum Dots for Room-Temperature Gas Sensors. *Nano-Micro Lett.* **2020**, *12*, 59. [[CrossRef](#)]
23. Zeng, Y.; Lin, S.; Gu, D.; Li, X. Two-Dimensional Nanomaterials for Gas Sensing Applications: The Role of Theoretical Calculations. *Nanomaterials* **2018**, *8*, 851. [[CrossRef](#)]
24. Wang, G.; Zheng, K.; Huang, Y.; Yu, J.; Wu, H.; Chen, X.; Tao, L.-Q. An investigation of the positive effects of doping an Al atom on the adsorption of CO₂ on BN nanosheets: A DFT study. *Phys. Chem. Chem. Phys.* **2020**, *22*, 9368–9374. [[CrossRef](#)] [[PubMed](#)]
25. Bhati, V.S.; Kumar, M.; Banerjee, R. Gas sensing performance of 2D nanomaterials/metal oxide nanocomposites: A review. *J. Mater. Chem. C* **2021**, *9*, 8776–8808. [[CrossRef](#)]
26. Mistry, K.; Ibrahim, K.H.; Novodchuk, I.; Ngo, H.T.; Imamura, G.; Sanderson, J.; Yavuz, M.; Yoshikawa, G.; Musselman, K.P. Nanomechanical Gas Sensing with Laser Treated 2D Nanomaterials. *Adv. Mater. Technol.* **2020**, *5*, 2000704. [[CrossRef](#)]
27. Lin, S.; Ye, X.; Johnson, R.S.; Guo, H. First-Principles Investigations of Metal (Cu, Ag, Au, Pt, Rh, Pd, Fe, Co, and Ir) Doped Hexagonal Boron Nitride Nanosheets: Stability and Catalysis of CO Oxidation. *J. Phys. Chem. C* **2013**, *117*, 17319–17326. [[CrossRef](#)]
28. Huang, Y.; Yang, T.; Yang, L.; Liu, R.; Zhang, G.; Jiang, J.; Luo, Y.; Lian, P.; Tang, S. Graphene–boron nitride hybrid-supported single Mo atom electrocatalysts for efficient nitrogen reduction reaction. *J. Mater. Chem. A* **2019**, *7*, 15173–15180. [[CrossRef](#)]
29. Zhou, Y.G.; Yang, P.; Sun, X.; Wang, Z.G.; Zu, X.T.; Gao, F. First-principles study of the noble metal-doped BN layer. *J. Appl. Phys.* **2011**, *109*, 084308. [[CrossRef](#)]
30. Wan, Q.; Chen, X.; Gui, Y. First-Principles Insight into a Ru-Doped SnS₂ Monolayer as a Promising Biosensor for Exhale Gas Analysis. *ACS Omega* **2020**, *5*, 8919–8926. [[CrossRef](#)]
31. Wu, P.; Zhang, X.; Chen, D.; Tang, J. Adsorption of SF₆ Decomposed Products on ZnO-Modified C₃N: A Theoretical Study. *Nanoscale Res. Lett.* **2020**, *15*, 186. [[CrossRef](#)]
32. He, X.; Gui, Y.; Liu, K.; Xu, L. Comparison of sensing and electronic properties of C₂H₂ on different transition metal oxide nanoparticles (Fe₂O₃, NiO, TiO₂) modified BNNT (10, 0). *Appl. Surf. Sci.* **2020**, *521*, 146463. [[CrossRef](#)]
33. Khan, M.A.H.; Thomson, B.; Motayed, A.; Li, Q.; Rao, M.V. Functionalization of GaN Nanowire Sensors With Metal Oxides: An Experimental and DFT Investigation. *IEEE Sens. J.* **2020**, *20*, 7138–7147. [[CrossRef](#)]
34. Xia, S.-Y.; Tao, L.-Q.; Jiang, T.; Sun, H.; Li, J. Rh-doped h-BN monolayer as a high sensitivity SF₆ decomposed gases sensor: A DFT study. *Appl. Surf. Sci.* **2021**, *536*, 147965. [[CrossRef](#)]
35. Xiong, Z.; Zhong, L.; Wang, H.; Li, X. Structural Defects, Mechanical Behaviors, and Properties of Two-Dimensional Materials. *Materials* **2021**, *14*, 1192. [[CrossRef](#)]
36. Lee, C.W.; Suh, J.M.; Jang, H.W. Chemical Sensors Based on Two-Dimensional (2D) Materials for Selective Detection of Ions and Molecules in Liquid. *Front. Chem.* **2019**, *7*, 708. [[CrossRef](#)] [[PubMed](#)]
37. Hong, J.; Hu, Z.; Probert, M.; Li, K.; Lv, D.; Yang, X.; Gu, L.; Mao, N.; Feng, Q.; Xie, L.; et al. Exploring atomic defects in molybdenum disulphide monolayers. *Nat. Commun.* **2015**, *6*, 6293. [[CrossRef](#)] [[PubMed](#)]
38. Zhou, N.; Gan, L.; Yang, R.; Wang, F.; Li, L.; Chen, Y.; Li, D.; Zhai, T. Nonlayered Two-Dimensional Defective Semiconductor γ-Ga₂S₃ toward Broadband Photodetection. *ACS Nano* **2019**, *13*, 6297–6307. [[CrossRef](#)] [[PubMed](#)]

39. Jin, C.; Lin, F.; Suenaga, K.; Iijima, S. Fabrication of a Freestanding Boron Nitride Single Layer and Its Defect Assignments. *Phys. Rev. Lett.* **2009**, *102*, 195505. [[CrossRef](#)]
40. Si, M.S.; Xue, D.S. Magnetic properties of vacancies in a graphitic boron nitride sheet by first-principles pseudopotential calculations. *Phys. Rev. B* **2007**, *75*, 193409. [[CrossRef](#)]
41. Azevedo, S.; Kaschny, J.R.; de Castilho, C.M.C.; de Brito Mota, F. A theoretical investigation of defects in a boron nitride monolayer. *Nanotechnology* **2007**, *18*, 495707. [[CrossRef](#)] [[PubMed](#)]
42. Li, T.; Gui, Y.; Zhao, W.; Tang, C.; Dong, X. Palladium modified MoS₂ monolayer for adsorption and scavenging of SF₆ decomposition products: A DFT study. *Phys. E Low-Dimens. Syst. Nanostruct.* **2020**, *123*, 114178. [[CrossRef](#)]
43. Hou, W.; Mi, H.; Peng, R.; Peng, S.; Zeng, W.; Zhou, Q. First-Principle Insight into Ga-Doped MoS₂ for Sensing SO₂, SOF₂ and SO₂F₂. *Nanomaterials* **2021**, *11*, 314. [[CrossRef](#)] [[PubMed](#)]
44. Gui, Y.; Chen, W.; Lu, Y.; Tang, C.; Xu, L. Au Catalyst-Modified MoS₂ Monolayer as a Highly Effective Adsorbent for SO₂F₂ Gas: A DFT Study. *ACS Omega* **2019**, *4*, 12204–12211. [[CrossRef](#)]
45. Li, P.; Hong, Q.; Wu, T.; Cui, H. SOF₂ sensing by Rh-doped PtS₂ monolayer for early diagnosis of partial discharge in the SF₆ insulation device. *Mol. Phys.* **2021**, *119*, e1919774. [[CrossRef](#)]
46. Zhu, H.; Cui, H.; He, D.; Cui, Z.; Wang, X. Rh-doped MoTe₂ Monolayer as a Promising Candidate for Sensing and Scavenging SF₆ Decomposed Species: A DFT Study. *Nanoscale Res. Lett.* **2020**, *15*, 129. [[CrossRef](#)] [[PubMed](#)]
47. Gui, X.; Zhou, Q.; Peng, S.; Xu, L.; Zeng, W. Adsorption behavior of Rh-doped MoS₂ monolayer towards SO₂, SOF₂, SO₂F₂ based on DFT study. *Phys. E Low-Dimens. Syst. Nanostruct.* **2020**, *122*, 114224. [[CrossRef](#)]
48. Delley, B. From molecules to solids with the DMol3 approach. *J. Chem. Phys.* **2000**, *113*, 7756–7764. [[CrossRef](#)]
49. Zhou, K.; Ma, W.; Zeng, Z.; Chen, R.; Xu, X.; Liu, B.; Li, H.; Li, H.; Li, L. Waste biomass-derived oxygen and nitrogen co-doped porous carbon/MgO composites as superior acetone adsorbent: Experimental and DFT study on the adsorption behavior. *Chem. Eng. J.* **2020**, *387*, 124173. [[CrossRef](#)]
50. Zhang, D.; Yang, Z.; Li, P.; Pang, M.; Xue, Q. Flexible self-powered high-performance ammonia sensor based on Au-decorated MoSe₂ nanoflowers driven by single layer MoS₂-flake piezoelectric nanogenerator. *Nano Energy* **2019**, *65*, 103974. [[CrossRef](#)]
51. Wang, J.; Zhou, Q.; Zeng, W. Competitive adsorption of SF₆ decompositions on Ni-doped ZnO (100) surface: Computational and experimental study. *Appl. Surf. Sci.* **2019**, *479*, 185–197. [[CrossRef](#)]
52. Zhu, X.; Zhang, L.; Zhang, M.; Ma, C. Effect of N-doping on NO₂ adsorption and reduction over activated carbon: An experimental and computational study. *Fuel* **2019**, *258*, 116109. [[CrossRef](#)]
53. Maximoff, S.N.; Ernzerhof, M.; Scuseria, G.E. Current-dependent extension of the Perdew–Burke–Ernzerhof exchange-correlation functional. *J. Chem. Phys.* **2004**, *120*, 2105–2109. [[CrossRef](#)]
54. Cui, H.; Zhang, G.; Zhang, X.; Tang, J. Rh-doped MoSe₂ as a toxic gas scavenger: A first-principles study. *Nanoscale Adv.* **2019**, *1*, 772–780. [[CrossRef](#)]
55. Grimme, S. Semiempirical GGA-type density functional constructed with a long-range dispersion correction. *J. Comput. Chem.* **2006**, *27*, 1787–1799. [[CrossRef](#)] [[PubMed](#)]
56. Monkhorst, H.J.; Pack, J.D. Special points for Brillouin-zone integrations. *Phys. Rev. B* **1976**, *13*, 5188–5192. [[CrossRef](#)]
57. Cui, H.; Zhang, X.; Zhang, J.; Ali Mehmood, M. Interaction of CO and CH₄ Adsorption with Noble Metal (Rh, Pd, and Pt)-Decorated N₃-CNTs: A First-Principles Study. *ACS Omega* **2018**, *3*, 16892–16898. [[CrossRef](#)] [[PubMed](#)]